Nanoscale Advances

ROYAL SOCIETY OF CHEMISTRY

PAPER

View Article Online
View Journal | View Issue

Cite this: *Nanoscale Adv.*, 2025, **7**, 8001

Polycaprolactone/chitosan core–shell nanoparticles for the acceleration of second-degree burn healing in CD1 mice

Alaa H. Saleh,[ab] Abeer M. Badr,*[a] Zeinab A. Muhammad,[c] Magdi E. A. Zaki,[d] Asmaa Abdel Kader,[a] Noha A. Mahana[a] and Ahmed S. Abo Dena *[ce]

Received 22nd April 2025
Accepted 22nd September 2025

DOI: 10.1039/d5na00391a

rsc.li/nanoscale-advances

Burn injuries are a major global health problem, and finding treatments for them is critical. Therefore, we aimed to design a drug delivery formulation for tea-tree oil comprising polycaprolactone/chitosan core–shell nanoparticles in order to accelerate the wound healing process in second-degree burns induced in CD1 mice. The present work is a continuation of our previously reported results on the antimicrobial and anti-inflammatory activity of the suggested nanomaterial. The nanoparticles (NPs) were optimized and characterized using FTIR spectroscopy, electron microscopy, dynamic light scattering, and zeta potential measurement. The investigations revealed that the best NP composition is 2 : 1 (PCL/CS, w/w), which showed an average particle size of 10.1 nm and a spherical core–shell structure. The nano-formulation was applied to burnt CD1 mice and showed a significant improvement in healing rate (21 days). Immunological analyses showed a significant increase in IL-13 and TNF-α levels. The immune response was enhanced in the early stages of burns, as revealed by the presence of $CD8^+$ T-cell subsets being more than the $CD4^+$ T-cells. Histological examination of burn areas showed healthy skin with a normal epidermal layer, newly formed blood capillaries, no scar formation, and apparently healthy hair follicles. TTO-loaded PCL/CS NPs provide a novel nanomaterial-based treatment for second-degree burns that can accelerate the wound healing process and prevent skin deformations *via* inducing tissue regeneration.

Introduction

Burns affect more than 6.6 million people worldwide, and they are among the most prevalent injuries that cause 1% of overall deaths.[1] Burn injuries are classified according to their severity, and they are the most destructive type of trauma that affects human life because they cause systemic damage and alter homeostasis.[2–4] Several factors lead to burns such as electricity, chemicals, high temperature, radiation and friction.[3] However, heat from hot liquids, fire or solids causes the most dangerous burn injuries. Burns can lead to necrosis in different skin layers, which act as the primary physiological barrier that protects deep layers from damage. The degree of damage is affected by temperature, period of exposure and the causative agent's energy transmission.[5] Burns may also be classified based on their size and depth. First-degree burns affect the uppermost layer of the skin (*i.e.*, the epidermis) only, so they are called superficial burns. In this case, the skin turns red, and the pain is only felt for a short period of time. Second-degree burns lead to the separation of the epidermis from its underlying layer (*i.e.*, the dermis), causing blisters, discomfort, and redness. These burns only affect the epithelium, sparing the dermis, and may result in local necrosis.[6] Third-degree burns are total-thickness injuries that impact the entire dermis. Because the nerve endings in the dermis are damaged, pain is not one of the manifestations of this kind of burn. Third-degree burns must be protected from infection, and if they are extremely small, surgical care might be needed. Fourth-degree burns typically result in the loss of the burnt area and the damage might extend to the underlying muscles or bones.[2,7]

Second-degree burns affect the epidermis and the papillary dermis, as mentioned above. They are partial-thickness burns that may leave scars but do not need surgery. These burns are weepy, painful, and necessitate the use of wound dressings during the course of treatment. Deep second-degree burns are less painful (owing to the partial destruction of the pain receptors), drier, require surgery and lead to scar formation. This kind of burn mainly influences the epidermis and the reticular dermis.[6,8] In this case, the burns are soft, wet, and blanch upon contact. They could be due to exposure to hot

[a]*Zoology Department, Faculty of Science, Cairo University, Giza 12613, Egypt*
[b]*Basic Science Department, Faculty of Physical Therapy, Egyptian Chinese University (ECU), Cairo, Egypt*
[c]*Pharmaceutical Chemistry Department, Egyptian Drug Authority (EDA) (Former National Organization for Drug Control and Research, NODCAR), Giza, Egypt*
[d]*Department of Chemistry, Faculty of Science, Imam Mohammad Ibn Saud Islamic University (IMSIU), Riyadh 11623, Saudi Arabia*
[e]*Nanomedicine Laboratories, Centre for Materials Science (CMS), Zewail City of Science and Technology, Egypt. E-mail: ahmed_said5899@yahoo.com; aabdelmawgoud@zewailcity.edu.eg*

surfaces, flames or hot liquids. The majority of second-degree burns require extended hospital stays, and the recovery is relatively difficult.[9,10]

Tea-tree oil (TTO), also known as *Melaleuca alternifolia* oil, is made from the leaves of the native Australian evergreen tea tree (a member of the Myrtaceae family) *via* steam-distillation. Along with other *Melaleuca* species, the leaves and branches of *M. alternifolia* have many essential oils, and could adapt to different climatic conditions. TTO is a volatile essential oil well known for its antibacterial, anti-inflammatory, antioxidant and anticancer activities.[11–13] TTO and terpinen-4-ol concentrations must be greater than 30%, while those of 1,8-cineole must be less than 15% based on the International Organization for Standardization (ISO) 4730 criteria. The mechanism of action for terpinen-4-ol is *via* regulating plasma extravasation and vasodilation. It also inhibits the synthesis of tumour necrosis factor (TNF), prostaglandin E2, interleukin-1 (IL-1), IL-8, and IL-10. Terpinen-4-ol and alpha-terpineol are two of the water-soluble components that inhibit superoxides of oxygen species through monocytes rather than by neutrophils.[14,15] According to the above-mentioned information, TTO is therefore widely used to treat burns, acne, wounds and fungal infections.[16]

Poly(ε-caprolactone) (PCL) is a common synthetic, polycrystalline, biodegradable and biocompatible polymer extensively employed in the fabrication of nano-drug delivery systems. Moreover, chitosan (CS) is a natural polysaccharide that is effective on large open wounds by promoting re-epithelialization and regeneration of the granular layer.[17,18] CS also exhibits many other properties such as antibacterial, biodegradability, biocompatibility, antifungal, antitumor and haemostatic properties. In the literature, it was employed in dressings and nanofibers to treat burn wounds. Recently, nanozymes and other materials were employed in the treatment of burn exacerbations such as microbial infections by antibiotic-resistant bacteria and muscle loss.[19–22]

In wound healing applications, combining PCL and CS may improve their properties such as water conservation, suitable degradation rate, and vascularization.[23] The present study is a continuation of our previous study published elsewhere.[24] Here, we propose the use of PCL/CS core–shell nanoparticles (NPs) for the topical delivery of TTO to accelerate wound healing in second-degree burns in CD1 mice. We hypothesize that the incorporation of a small amount of TTO in the water-soluble CS shell will relieve wound inflammation (due to TTO's anti-inflammatory activity) and prevent bacterial growth (due to CS's antibacterial activity), and then the prolonged release of TTO from the PCL core will further maintain the anti-inflammatory, antibacterial and analgesic actions, and induce wound healing and cell proliferation at the burn site. The PCL core was selected because of its hydrophobic nature which permits the loading of a high amount of the oil to be delivered. Moreover, CS was selected as a thin shell due to its well-known antimicrobial activity which will be exerted at the burn site before the release of the loaded TTO from the core. The proposed core–shell NPs will be applied topically with the aid of a cream formulation. It is supposed that the core–shell structure is crucial here because the outer shell layer (CS layer) will act as an antibacterial layer in the first stage to prevent the delay of the healing process due to infection. On the other hand, this layer forms a hydrogel which swells in the presence of moisture and allows for the sustained release of TTO from the PCL core. The main objective of the present study is to find an effective and rapid treatment for second-degree burns, and help in reducing the cost of hospitalization and medical care. This study introduces a novel drug delivery system using tea-tree oil-loaded polycaprolactone/chitosan core–shell nanoparticles optimized at a 2 : 1 ratio, which significantly accelerates healing of second-degree burns in CD1 mice by enhancing early immune response and promoting tissue regeneration without scar formation.

Experimental

Materials

Poly(ε-caprolactone) (PCL) (linear, molecular weight: ~45 000 g mol^{-1}) and low-molecular-weight poly vinyl alcohol (PVA) were purchased from Sigma-Aldrich (St. Louis, MO, USA). Chitosan (CS) powder (Acros Organics, molecular weight = 600 000–800 000 g mol^{-1}) (Belgium) was used for core–shell nanoparticle preparation. Tea-tree oil (TTO) was obtained from Nefertari (Egypt). Dichloromethane (DCM) was supplied by Diachem Chemicals, Egypt. Glacial acetic acid was obtained from Piochem (Egypt). Deionized water was obtained from a laboratory water deionizer, and was used for solution preparation throughout the work. All reagents were of analytical grade and were used without any further purification.

Synthesis of PCL/CS core–shell NPs

The proposed PCL/CS core–shell NPs were synthesized *via* a nanoemulsion-solvent evaporation method. The preparations were divided into four ratios of CS to PCL, namely 2 : 1, 1 : 1, 2 : 3, and 1 : 2 (w/w), respectively. TTO-loaded PCL/CS core–shell NP preparation was achieved as follows. For the 1 : 1 (PCL/CS) ratio, 0.2 g of PCL was dissolved in 2.0 mL of DCM, and then 0.07 mL of TTO was added. The obtained mixture was poured into 23 mL of 2% acetic acid solution containing 0.2 g of CS and 1.0 g of PVA dissolved in 10 mL of deionized water. This mixture was vigorously stirred until the organic solvent was totally evaporated, and a suspension was formed. The remaining ratios (1 : 2, 3 : 2 and 2 : 1 (PCL/CS)) were prepared by varying the weights of CS. The procedure to prepare plain PCL/CS core–shell NPs was the same as the above-mentioned procedure but without adding TTO. The synthesis of TTO-loaded core–shell NPs is illustrated in Fig. 1.

Cream preparation

The cream formulation (100 g) was prepared using the oil-in-water method with minor modifications.[25] The oil phase was composed of 10 g of stearic acid, 10 g of cetyl alcohol, 2 g of bee wax, and 5.48 mL of almond oil. These components were heated to 75 °C and mixed well during heating. The aqueous phase was composed of 88.8 mL of deionized water, 3.97 mL of glycerine

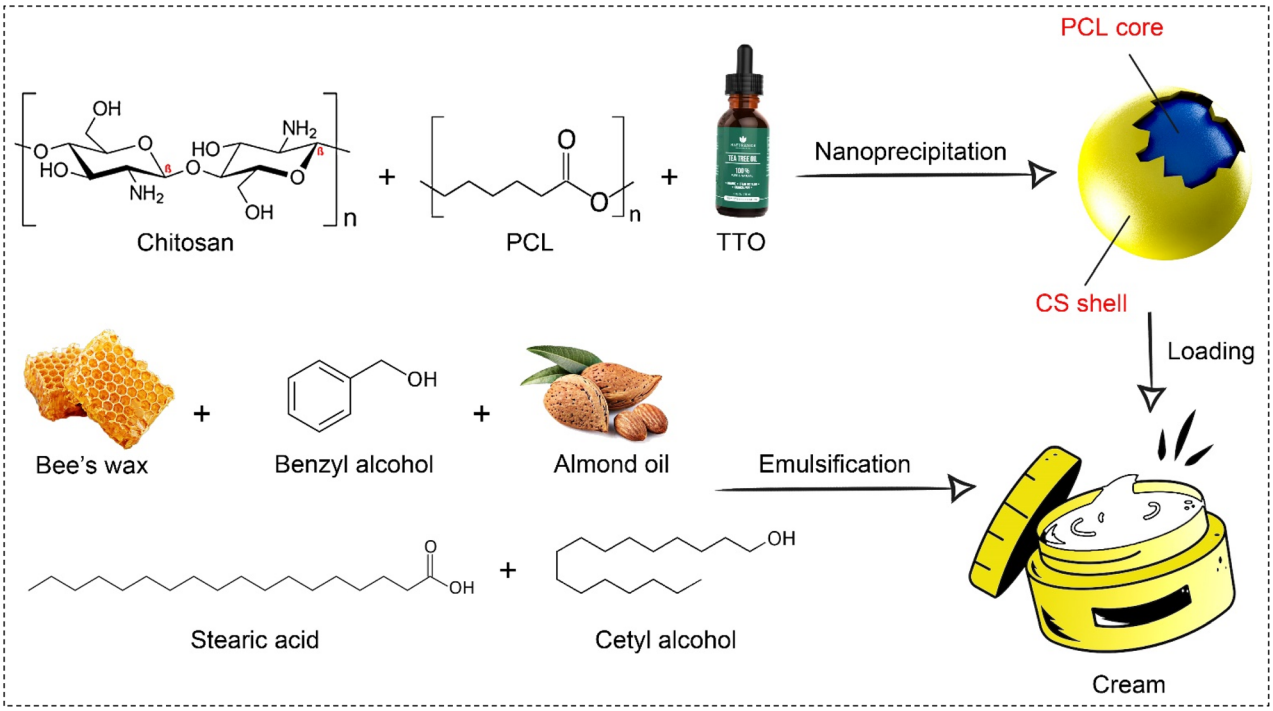

Fig. 1 A comprehensive diagram illustrating the general outline of the synthesis of the TTO-loaded core–shell nanoparticles and the cream formulation.

and 1.69 mL of benzyl alcohol. The components of the aqueous portion were heated to 75 °C and mixed well during heating. Thereafter, the aqueous phase was poured into the oil phase with continuous stirring until the cream was formed. To prepare the NP-containing cream for wound treatment, 10% (w/w, with respect to the cream weight) of pure TTO, plain PCL/CS core–shell NPs, or TTO-loaded PCL/CS core–shell NPs were mixed with the cream and stored for subsequent application.

Fourier-transform infrared spectroscopy

Fourier-transform infrared (FTIR) absorption spectroscopy was used to confirm TTO loading onto the PCL/CS core–shell NPs. The FTIR spectra of TTO-loaded PCL/CS NPs, pure PCL, pure CS and pure TTO were recorded in the mid-IR region over the wavenumber window of 400–4000 cm^{-1} using the KBr-disc method and an FTIR spectrometer, model Nicolet 6700 (USA).

Transmission electron microscopy

A transmission electron microscope (TEM) (JEOL GEM-1010, Tokyo, Japan) was used at 80 kV to investigate the morphology of the PCL/CS core–shell NPs at the Regional Centre for Mycology and Biotechnology (RCMB), Al-Azhar University, Egypt. A drop of an aqueous suspension of the NPs was applied to the carbon-coated copper grids (CCG), and then the CCGs were allowed to dry at room temperature prior to imaging.

Dynamic light scattering and zeta potential

The prepared plain and TTO-loaded PCL/CS core–shell NPs were analysed for their particle size distribution and polydispersity index at a fixed angle of 173° at room temperature by photon correlation spectroscopy using a dynamic light scattering (DLS) particle size analyser (Zetasizer Nano ZN, Malvern Panalytical Ltd, United Kingdom). The samples were analysed in triplicate. The same instrument was used to determine the zeta potential (ZP) of the prepared NPs.

In vivo experiments

Ethical approval. All animal experiments were approved by the Cairo University Institutional Animal Care and Use Committee with permission number CU/I/F/56/21.

Experimental design. A pre-calculated number of CD1 albino mice (weighing 20–23 g) was used in the animal model experiments. The animals were obtained from the National Organization for Drug Control and Research (NODCAR), Giza, Egypt. In order to induce the second-degree burn, the Priya method was applied.[26] The dorsal skin of the mice was shaved and burnt by a sterile metal plate of 1.0 cm diameter. All these procedures were performed under general anaesthesia using ketamine (50 mg kg^{-1}) and xylazine (10 mg kg^{-1}) *via* the intraperitoneal injection route. The animal groups were divided into six groups (5 animals per group) as shown in Table 1. For the topical treatment using the cream formulation, 500 mg of the plain or loaded cream formulation were applied topically once daily over the burn area for 21 days. The animals were euthanized after 21 days of treatment, and skin, blood and spleen samples were collected for assessment.

Macroscopic observations. The optimal temperature for inducing the second-degree burn was 120 °C for 3 s. Digital

Table 1 Animal groups used in the animal model experiments in the present study

Group code	Group name	Treatment
G1	Normal animals (negative control)	Normal mice (unburnt and untreated)
G2	Positive control	Burnt untreated mice
G3	TTO	Burnt mice topically treated with pure TTO
G4	Plain	Burnt mice treated with a cream formulation containing plain PCL/CS core–shell NPs
G5	Cream	Burnt mice treated with a pure cream formulation
G6	Whole formulation	Burnt mice treated with TTO-loaded PCL/CS core–shell NPs

images of the burn area were captured using a digital camera, while positioning a ruler adjacent to the wound to measure the diameter of the burn area on days 1, 3, 5, 8, 10, 15, and 21. The wound diameter was measured using the ImageJ image analysis software.

Enzyme-linked immunosorbent assay (ELISA). Sera were collected from all mice 3 days after receiving the dose of treatment, and then tested for cytokine levels. Levels of the mouse cytokines that play a main role in wound healing; namely, TNF-α and IL-13, were quantified by sandwich capture enzyme-linked immunosorbent assay (sELISA) kits (Cloud-Clone Corp, USA) according to the instructions of the manufacturer.

Flow cytometry. The collected spleen samples from all animal groups were squeezed gently in PBS buffer (pH 7.4) with a dilution factor of 1 : 10 by a syringe piston. The cells were suspended in 1.0 mL of the PBS solution and centrifuged for 10 min at 1200 rpm. After discarding the supernatants, the pellets were resuspended in 200 μL of the PBS solution and gently vortexed. Subsequently, 100 μL of the suspended cells were put into the reaction tubes. Monoclonal antibodies were added as follows: 7.0 μL of $CD8^+$ and 5.0 μL of $CD4^+$. The reaction tubes containing 100 μL of the cell suspensions received the antibody volumes, whilst the control tube remained empty of antibodies. After incubation in the dark for 15 min, 2.0 mL of the lysing buffer was added to each reaction tube, and then the tubes were incubated in the dark for 10 min. The tubes were then centrifuged for 3 min, the supernatants were discarded, and the cell pellets were washed with 1.0 mL of the PBS solution. After washing, the cell pellets were resuspended in 400 μL of the PBS solution for subsequent flow cytometry analysis using BD FACS™ Lysing Solution (BD Biosciences, USA).

Histological examination. Skin tissue samples of each mouse were fixed in a neutral 10% buffered formaldehyde solution, and then embedded in paraffin. Four-micrometre sections were stained with haematoxylin/eosin (H&E) for histopathological examination. A system of scoring for burn wounds was used based on re-epithelialization as follows: score 0, absence of epithelialization; score 1, poor epidermal organization; score 2, incomplete epidermal organization; score 3, moderate epithelial proliferation; score 4, complete epidermal remodelling. The same scoring system was used based on granulation (score 0, immature and inflammatory tissue; score 1, thin immature and inflammatory tissue; score 2, moderate remodelling tissue; score 3, thick granulation layer; score 4, complete tissue organization. Similarly, the samples were scored according to the number of inflammatory cells as follows: score 0, 13–15 inflammatory cells; score 1, 10–13 inflammatory cells; score 2, 7–10 inflammatory cells; score 3, 4–7 inflammatory cells; score 4, 1–4 inflammatory cells. Finally, a similar scoring system was used to indicate the degree of angiogenesis as follows: score 0, absence of angiogenesis; score 1, 1–2 vessels in site; score 2, 3–4 vessels in site; score 3, 5–6 vessels in site; score 4, more than 7 vessels in site).[27]

Statistical analysis. The obtained data were expressed as mean (M) ± standard error of the mean (SEM). All experiments were repeated at least three times. To determine the statistical significance of the differences between the experimental and control groups, Statistical Package for the Social Sciences (SPSS) version 24.6 was used. Statistical significance was accepted at P values less than 0.05 by using the Student's t-test.

Results

FTIR spectroscopy

The FTIR spectra of pure TTO, plain PCL/CS core–shell NPs, and TTO-loaded PCL/CS core–shell NPs were recorded over the spectral window of 400–4000 cm^{-1}. The observed infrared absorption bands are shown in Fig. 2A.

For pure TTO, absorption bands are observed at 2965 cm^{-1} (C–H stretching) and 1127 cm^{-1} (C–O stretching), corresponding to the tertiary alcohol of both terpenes and terpineol. In addition, the bands appearing at 910, 889, 864, and 799 cm^{-1} correspond to the C=C bending of terpinene-4-ol,[28] and those observed at 830, 815, and 780 cm^{-1} correspond to the C=C bending of γ-terpinene.[29] The C=O peak of the PCL/CS NPs can be observed at 1721 cm^{-1}.[30] Most of the above-mentioned infrared absorption bands of TTO can be observed in the FTIR spectrum of TTO-loaded PCL/CS core–shell NPs. For instance, the band at 2965 cm^{-1} (C–H stretching of TTO) is obvious in the FTIR spectrum of the TTO-loaded PCL/CS core–shell NPs. Moreover, the band observed at 1721 cm^{-1} (C=O of PCL/CS) is also found in the same spectrum. Therefore, the FTIR results confirm the loading of PCL/CS core–shell NPs with TTO.

The FTIR spectrum of the cream formulation showed an absorption band at 3304 cm^{-1}, which may be attributed to the O–H stretching of cetyl alcohol, benzyl alcohol and glycerine. In addition, the bands observed at 2914 and 2847 cm^{-1} are assigned to C–H stretching of the methyl and methylene groups, respectively. The carbonyl group of the bee's wax appeared as a sharp absorption band at 1735 cm^{-1}. The band observed at

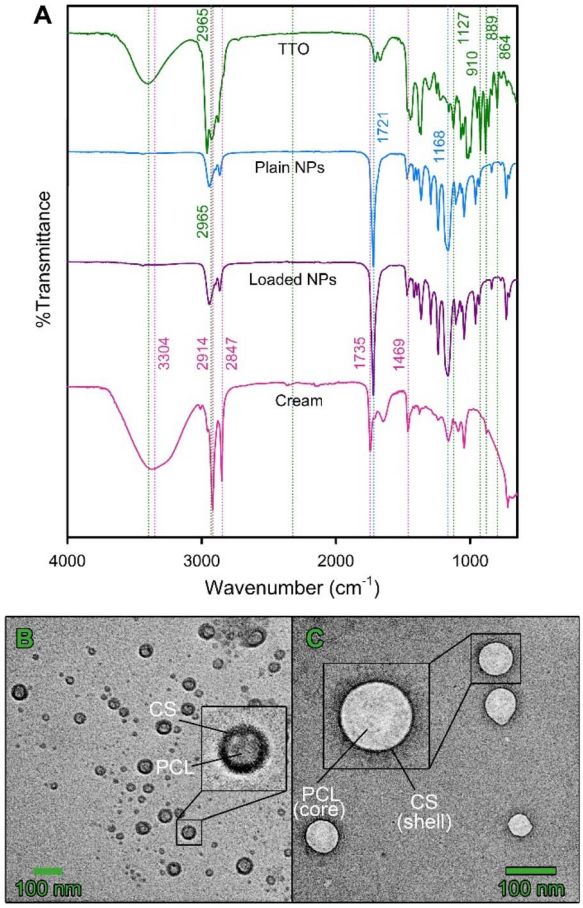

Fig. 2 (A) FTIR absorption spectra of pure TTO, plain PCL/CS core–shell NPs, and TTO-loaded PCL/CS core–shell NPs; (B) TEM image of TTO-loaded PCL/CS core–shell NPs; (C) TEM image of plain PCL/CS core–shell NPs.

1469 cm^{-1} may be assigned to the bending of the $-CH_2$ groups of the aliphatic chains.

TEM imaging

TEM was used to observe the morphological characteristics of the plain and TTO-loaded PCL/CS core–shell NPs. Fig. 2B and C depict the TEM images of plain and TTO-loaded NPs, respectively. The NPs appear spherical in shape and show a homogeneous size distribution. The PCL and TTO (Fig. 2B) appear in the core, while CS appears as a thin shell around it. The CS shell is very obvious in both the plain and TTO-loaded NPs. It is worth mentioning that the NP size in the case of TTO-loaded PCL/CS core–shell NPs is less than 100 nm, which is slightly less than that of the plain PCL/CS core–shell NPs. This reduction in the NP size may be attributed to the presence of TTO. No aggregates could be observed, indicating the good dispersibility of the NPs in the sample suspension.

DLS and ZP measurements

The zeta sizer apparatus was used to determine the size distribution and the ZP of plain and TTO-loaded PCL/CS core–shell NPs. Table 2 shows the measured ZP values and the particle size distribution of PCL/CS core–shell NPs comprising different ratios of PCL and CS. The ZP results indicate that all NPs have positive ZP values. The highest ZP value (52.1 ± 2.00 mV) was observed in the case of TTO-loaded PCL/CS core–shell NPs with a 2 : 1 (PCL/CS) ratio (NP4). This result reflects the high stability of the NP suspension containing NP4. Accordingly, the 2 : 1 (PCL/CS) particle composition was selected as the best, and was used for the preparation of the plain and TTO-loaded PCL/CS NPs throughout the rest of the experiments. It is worth mentioning that NP4 showed a particle size of 10.1 nm which is the smallest obtained particle size amongst all the TTO-loaded NPs. Furthermore, NP5 (plain PCL/CS core–shell NPs with 2 : 1 PCL/CS ratio) showed a particle size distribution of 5.6 nm.

Table 2 Zeta potential and particle size of PCL/CS core–shell NPs comprising different ratios of PCL and CS[a]

	Composition				
Code	PCL	CS	PVA	ZP (mV)	Size (nm)
NP1	1	2	1	31.0 ± 0.98	50.5
NP2	1	1	1	45.7 ± 0.23	17.1
NP3	2	3	1	44.1 ± 1.99	23.6
NP4	2	1	1	52.1 ± 2.00	10.1
NP5	2	1	1	47.2 ± 1.15	5.60

[a] NPs (1–4): TTO-loaded; NPs 5: plain.

Regarding the stability of the cream formulation, it is worth mentioning that the stability of the cream formulation was stable for 20 days at room temperature with no observable phase separation or viscosity change.

Macroscopic observations of burn areas

The burn wound diameter was monitored in all animal groups (Fig. 3). On day 1 of burn induction, the diameter was 10 mm. After 3 days, G6 animals showed a diameter of 10 mm, while in the case of G2, G3, G4, and G5 animals, the wound diameter showed an obvious increase. By day 5, the diameter of the wound in G6 animals became smaller (*ca.* 9 mm). Furthermore, on day 8, the wound diameter remained at 9 mm in G6 when compared to G2 whose burn diameter reached 15.45 mm. The healing progress appeared on day 10, when the wound diameter of G6 animals was found to be 8.34 mm, while in G2 it was found to be 14.76 mm. Finally, after 21 days, the wound diameter was 4.8 mm in G6 animals, thus indicating the successful acceleration of wound healing by the TTO-loaded PCL/CS core–shell NPs. All animal groups showed a reduction in the wound diameter by day 10. For instance, G3 and G4 demonstrated a wound diameter of 8.41 and 9.36 mm, respectively. It is worth mentioning that G3 animals showed the smallest wound diameter (2.94 mm) on day 21, followed by G6 animals (4.8 mm). This indicates the potency of TTO in accelerating the wound healing process based on wound diameter measurement. However, wound diameter measurement alone is not enough to govern the efficacy of the proposed nanoformulation, and further assessment methods (*e.g.*,

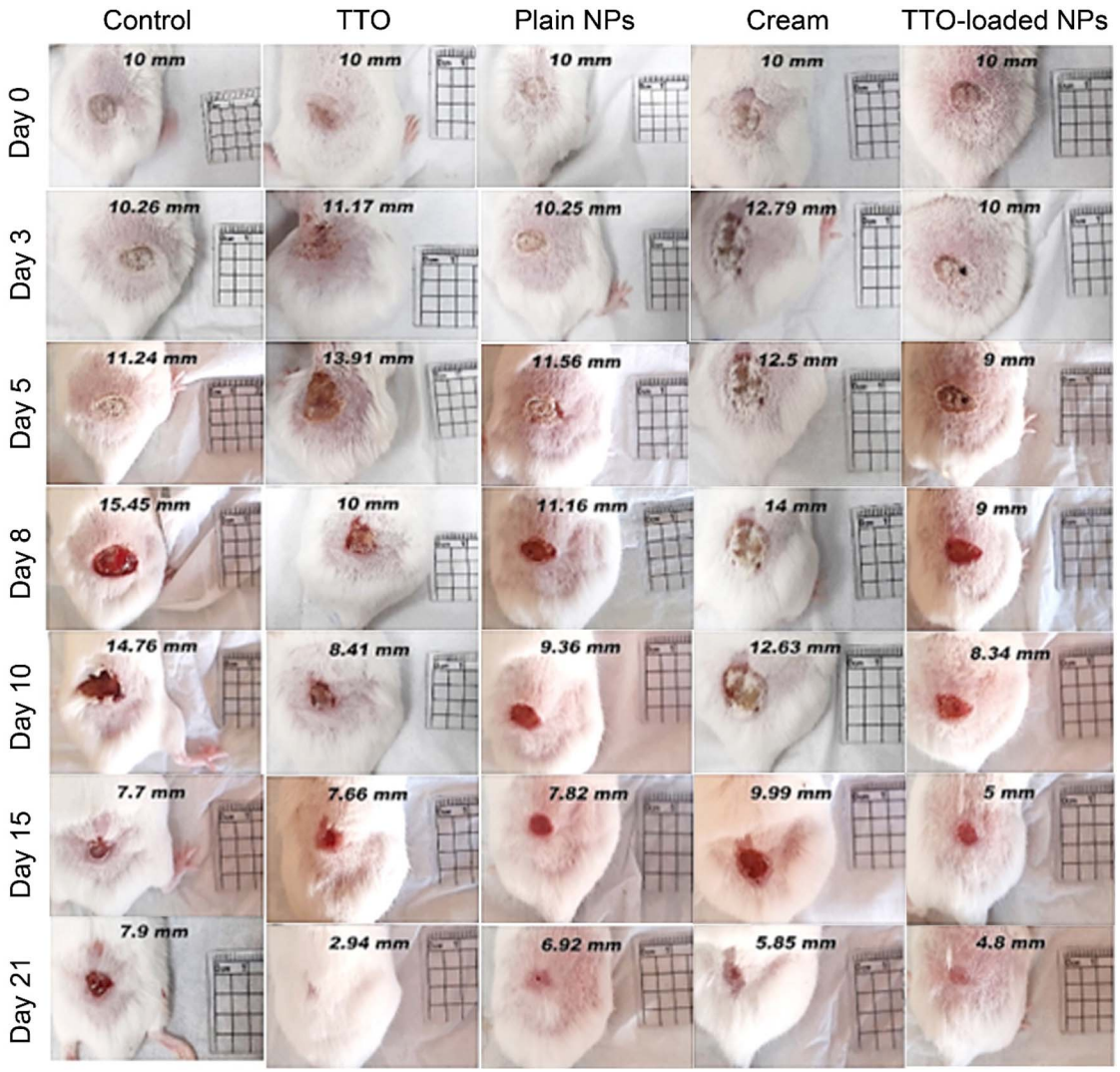

Fig. 3 Macroscopic appearance of the burn diameter in G2, G3, G4, G5 and G6 animal groups over a period of 21 days. The burn diameter is depicted in millimetres over each digital image. A ruler is placed beside each mouse to show the scale.

histopathological and immunological investigations) must be performed. The results of these investigations are summarized in the following parts of this section.

Cytokine profiles

The levels of IL-13 and TNF-α after 21 days of treatment following burn induction are shown in Fig. 4. G6 animals showed a significant increase in IL-13 levels (84.06 ± 3.95 pg mL^{-1}, $P < 0.05$) compared to G2 animals (67.22 ± 4.46 pg mL^{-1}). In addition, IL-13 levels were significantly decreased in G2 animals (67.22 ± 4.46 pg mL^{-1}, $P < 0.05$), compared to G1 animals (87.62 ± 4.56 pg mL^{-1}, $P < 0.05$). The level of IL-13 in G3 animals did not show a significant difference when compared with G2 animals. G5 and G2 animals showed a significant decrease in IL-13 levels compared to G1 animals.

The pro-inflammatory cytokine, TNF-α, showed the highest level in G6 animals (994.28 ± 85.87 pg mL^{-1}, $P < 0.05$) compared G1 and G2 animals. Moreover, G3 and G4 animals showed 622.35 ± 34.154 and 956.56 ± 62.59 pg mL^{-1} ($P < 0.05$) of the TNF-α cytokine, respectively. These levels were significantly different from those of G1 and G2 animals. However, animals of G4 showed intermediate levels of TNF-α (956.56 ± 62.59 pg mL^{-1}) between G6 and G3.

Flow cytometry

$CD4^+$ cells. The histogram of the $CD4^+$ expression is depicted in Fig. S1 in the SI. The percentage frequency of parent $CD4^+$ expression in G6 animals was low (11.8 ± 0.88%) and close to that of G1 animals. It is observed that the mice treated with TTO-loaded PCL/CS core–shell NPs showed significantly the lowest percent compared to G3 and G4 animal groups. In addition, G1 mice demonstrated a $CD4^+$ expression percentage of 9.43 ± 0.84%. Furthermore, it is worth mentioning that the mean percentage of $CD4^+$ expression in G6 animals was significantly higher ($P < 0.05$) than that of the normal mice in G1. The $CD4^+$ expression in the studied animal groups is in the order: G1 < G2 < G6 < G4 < G3 < G5 as shown in Fig. 5A.

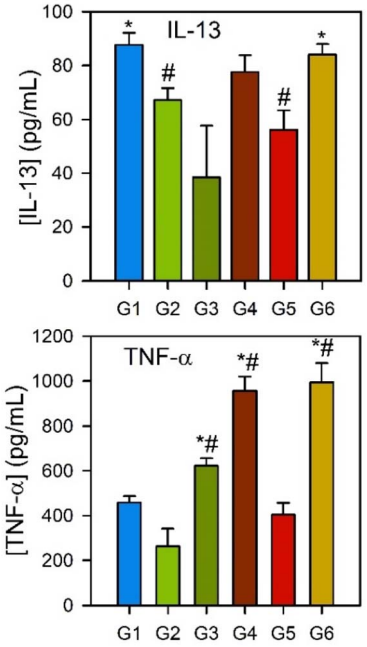

Fig. 4 Levels of IL-13 and TNF-α assayed in skin samples obtained from G1, G2, G3, G4, G5 and G6 animals. Values are expressed as mean ± SEM ($n = 3$). The symbol # indicates a significant difference ($P < 0.05$) compared to G1 animals, and * indicates a significant difference ($P < 0.05$) compared to G2 animals.

$CD8^+$ cells. The $CD8^+$ expression histogram is presented in Fig. S2. G6 animals showed a reduction in $CD8^+$ expression (18.4 ± 6.39%) compared to G3 (20.5 ± 1.55%), G4 (48.96 ± 7.78%) and G5 (28 ± 3%) animal groups. Meanwhile, the percentage frequency of parent $CD8^+$ in G6 was closer to that of G1 (15.53 ± 6.14%) than that of G2 (14.56 ± 7.31%). However, the $CD8^+$ frequency was significantly ($P < 0.05$) increased in G4 mice compared to G2. Moreover, the animals of G3 demonstrated a high $CD8^+$ expression (20.5 ± 1.55%) compared to G2, but with no significant difference (Fig. 5B).

$CD4^+/CD8^+$ cells. The $CD4^+/CD8^+$ dot plot is shown in Fig. S3, where each quadrate represents the cell proportions after gating. In all animal groups, most of the cells are represented in the double negative for both CD4 and CD8 ($CD4^-/CD8^-$). Mice of G6 showed double negative ($CD4^-/CD8^-$) close to G1 and G2 animals, while G3, G4 and G5 mice showed a highly double positive cell expression. In Fig. 5C, the animals of G6 showed the lowest percentage frequency of the parent of $CD4^+/CD8^+$ (0.5 ± 0.057%) with a significant difference compared to G1 normal mice. In addition, G4 animals showed a significant difference in $CD4^+/CD8^+$ expression (0.96 ± 0.08%) compared to G1 and G2 animals. The percentage frequency of the parent of $CD4^+/CD8^+$ in G5 was significantly higher (1.26 ± 0.28%) than those of G1 and G2.

Histological examination. The histological results (Fig. 6) of G1 animals showed an intact skin structure comprising both the epidermis and the dermis. The control group (G2) revealed second degree burns with thermal degenerative changes in the epidermal layer. These changes included vacuolation of prickle cells with vesicle formation and haemorrhagic patch formation in the hyaline layer of the epidermis. Dermal oedema was also observed, along with dispersed collagen fibres and infiltration of mononuclear inflammatory cells and mast cells in the dermis. Additionally, some hair follicles showed different degenerative changes. Mice of G6 showed good response to skin healing, as evidenced by the apparently healthy epidermis and dermis. Moreover, newly formed blood capillaries, apparently healthy hair follicles, and normal collagen fibres were noticed in the dermis. G4 animals revealed healing with scar formation in the superficial epidermal layer. Furthermore, thinning and deformation of the epidermal layer were observed in almost all skin parts with mild regeneration in hair follicles, congestion of the dermal blood vessel and moderately dispersed collagen fibres with severe mononuclear inflammatory cell infiltration. Meanwhile, mild vacuolation of prickle cells in the epidermal layer was also found.

For G3 animals, the skin showed an apparently healthy, yet thickened epidermal layer. Mildly dispersed collagen fibres, mild vacuole degeneration of the prickle cells and fine rete pegs (ridges), epithelial extensions projecting into the underlying connective tissue, were observed. Furthermore, there was a mild degeneration in the hair follicles and sebaceous glands. Regarding G5 animals, the skin showed a mild regeneration in the thinner epidermal layer. Moderate degenerative changes were observed in sebaceous glands and hair follicles with

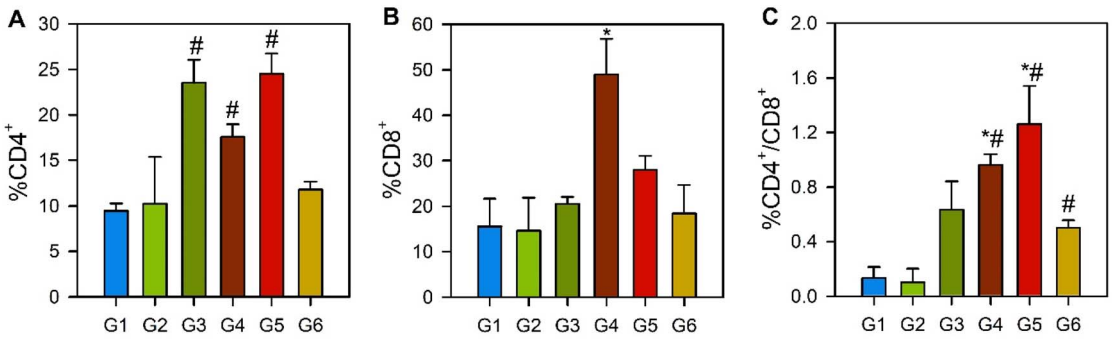

Fig. 5 Percentage frequency of $CD4^+$ (A), $CD8^+$ (B) and $CD4^+/CD8^+$ (C) cells in G1, G2, G3, G4, G5 and G6 animals. The symbol * indicates a significant difference ($P < 0.05$) compared to G2 animals, and # indicates a significant difference ($P < 0.05$) compared to G 1 animals. The experiments were performed in triplicate ($n = 3$).

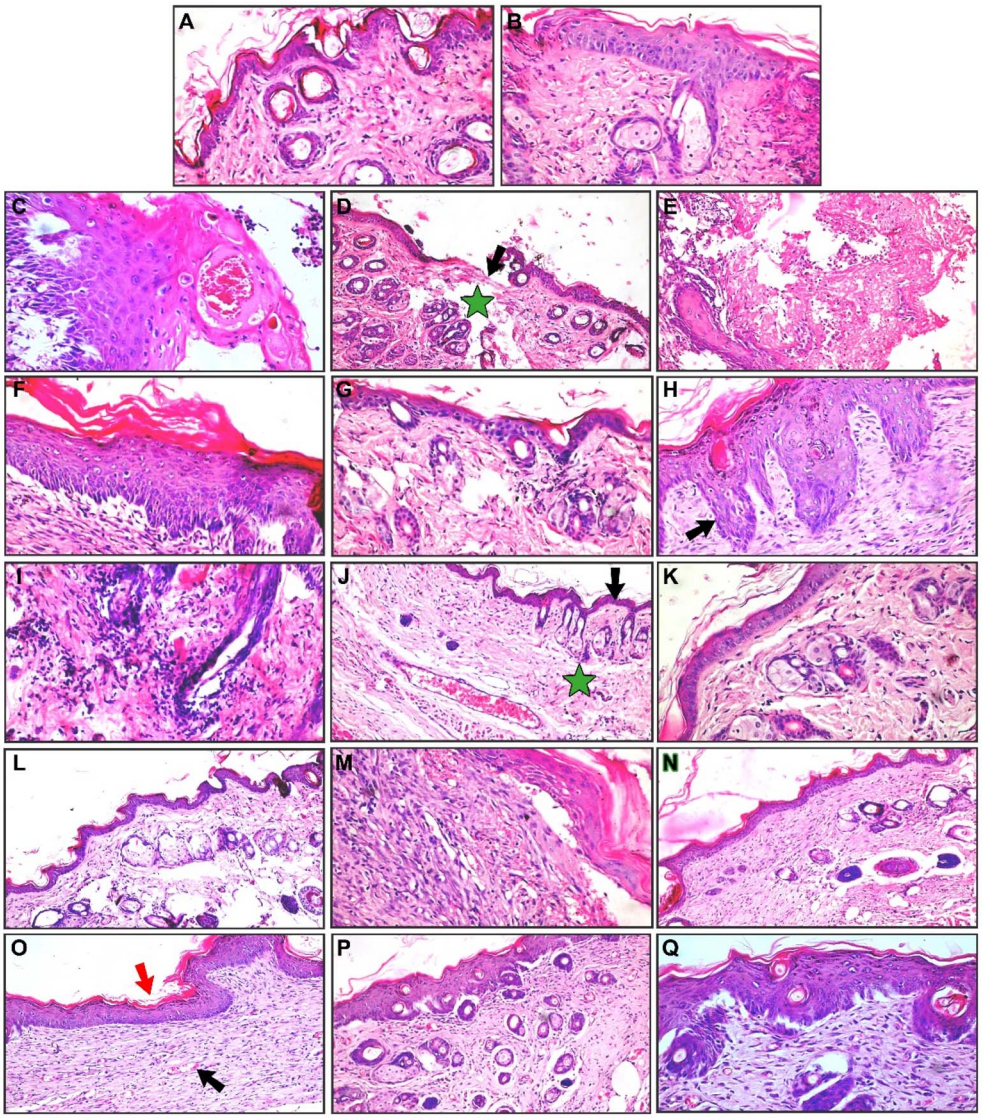

Fig. 6 Histopathological examination of skin stained with H&E. (A) and (B) normal skin structure of the epidermal layer and dermis (400×). (C) Skin from G2 showing vacuolar degeneration and vesicle in the prickle cell layer of the epidermis (400×). (D) Skin from G2 showing separation in the epidermal layer (arrow) with dermal oedema (star) (200×). (E) Skin from G2 showing burns with coagulative necrosis and dispersed collagen fibres and mononuclear inflammatory cell infiltration in the dermis (200×). (F) Skin from G3 showing apparently healthy skin with thickening of the epidermal layer and mildly dispersed collagen fibres (400×). (G) Skin from G3 showing the epidermal layer with fine rete ridges and few areas of dispersed collagen fibres (400×). (H) Skin from G3 showing rete pegs (ridges), the epithelial extensions that project into underlying connective tissue (arrow) (400×). (I) Skin from G4 showing dermis degeneration and coagulative necrosis of collagen fibres (400×). (J) Skin from G4 showing thinning of the epidermal layer with congestion of the dermal blood vessel (arrow) (200×). (K) Skin from G4 showing mild vacuolation of prickle cells of the epidermal layer (400×). (L) Skin from G5 showing mild regeneration of skin with a thinner epidermal layer (200×). (M) Skin from G5 showing response to healing (400×). (N) Skin from G5 showing apparently healthy structure (200×). (O) Skin from G6 showing apparently healthy skin with an apparently normal epidermal layer (red arrow) and newly formed blood capillaries and normal collagen fibres in the dermis (black arrow) (200×). (P) Skin from G6 showing apparently healthy skin with an apparently normal epidermal layer and dermis with newly formed blood capillaries and apparently healthy hair follicles were noticed (200×). (Q) Skin from G6 showing apparently healthy skin with an apparently normal epidermal layer and dermis with apparently healthy hair follicles (×400).

dispersed collagen fibres. Moreover, dermal haemorrhagic patches and mononuclear inflammatory cell infiltration were present. Fig. 7 shows that the animal groups can be arranged in the following order according to the used scoring system mentioned in the materials and methods section: G2 < G4 < G5 < G3 < G6, which means that the best healing was observed in G6 animals, and the worst was observed in G2 animals.

Discussion

Burns of the second degree are prevalent; however, these burns heal without the need for surgery. It is important to verify wound protection from infection, wound conversion and dehydration.[31] Developing PCL-based NPs has been described for improving drug encapsulation and release control. It was

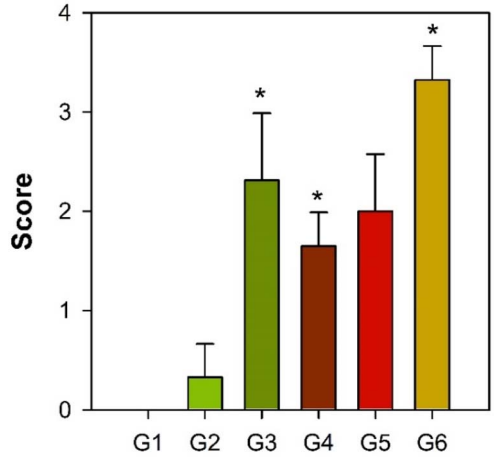

Fig. 7 Histological scores in G1, G2, G3, G4, G5 and G6 animals. Values are expressed as mean ± SEM (error bars, $n = 3$). The symbol * indicates a significant difference ($P < 0.05$) compared to G2 animals.

discovered that diffusion or matrix erosion are considered the principal mode of action for drug release in PCL nanomaterials.[32,33] There are many advantages for core–shell nanoformulations such as increasing encapsulant bioavailability, permitting improved chemical stability, reducing toxicity, increasing intracellular uptake, preventing aggregation and enhancing solubility.[34] Therefore, incorporating TTO in PCL/CS core–shell NPs is a promising approach for the delivery of TTO because it allows for TTO's sustained release and facilitates its penetration through the skin.[35] In the literature, PCL with CS nanofibrous scaffolds were developed as a wound dressing.[36] In the present study, FTIR absorption analysis confirmed the formation of PCL/CS core–shell NPs and proved that TTO was successfully encapsulated inside them. The presence of CS in the shell was confirmed and with the CS coating, a well-defined core–shell structure of TTO-loaded PCL/CS core–shell NPs was formed. The inner spherical shape was observed with the aid of TEM imaging; these results are in good agreement with those reported in recent studies.[37,38] The ZP values of the suggested TTO-loaded PCL/CS core–shell NPs herein agree with the results reported in the literature, that showed a positive ZP value for PCL with CS.[39] Since the ZP value of the PCL/CS core–shell NPs is higher than 30 mV, they are considered very stable in suspension.[39,40] This strong positive charge (which is attributed to the presence of the cationic CS polymer in the shell) might provide more potent antibacterial action.[41] For the TTO-loaded NPs with a 1 : 2 (PCL/CS) ratio, the ZP was 31.0 ± 0.98 mV. However, NPs containing a 1 : 1 (PCL/CS) ratio showed a ZP value of 45.7 ± 0.23 mV. Meanwhile, the NPs comprising a 2 : 3 (PCL/CS) ratio had a ZP value of 44.1 ± 1.99 mV. Moreover, plain NPs with a 2 : 1 (PCL/CS) ratio showed a ZP value of 47.2 ± 1.15 mV. Therefore, the suspensions of the NPs containing 1 : 2, 1 : 1, and 2 : 3 (PCL/CS) ratios were not very stable and showed aggregations. On the other hand, there was no aggregation in the suspension of the 2 : 1 (PCL/CS) TTO-loaded core–shell NPs.[38,42] Furthermore, the particle size analysis confirmed the encapsulation of TTO inside the PCL/CS core–shell NPs due to the increase in the particle size compared to that of the plain PCL/CS core–shell NPs. Based on the particle size and ZP measurements, the 2 : 1 (PCL/CS) ratio was selected for the fabrication of the TTO-loaded core–shell NPs.

It was reported that nanolipogels promote the release of TTO, and make it easier for it to penetrate and deposit in the skin layers; as a result, dermal repair/healing speeds up.[43] In another study, wound treatment with core–shell PCL/gelatine showed a mean wound closure of 85.9 ± 15.8%.[44] Therefore, TTO is a potential candidate that contributes to cell migration, and improves the process of wound closure with more than 70% in the present study. The lipophilicity of TTO enables it to enter the cell membrane. In addition, the physicochemical characteristics of oils help in preventing microbial invasion, stopping water loss, lowering colonization, and thus preventing wound infection.[45,46]

In the present study, the wound diameter in G6 animals decreased over 21 days, indicating accelerated wound healing. On the other hand, the burn size was increased in all other studied animal groups on day 3. In a previous study, PCL with ZnO NPs showed full wound healing on day 25 after wound induction, possibly due to cell migration and proliferation.[47] For treating burn wounds in the backs of rats, CS/polyethylene oxide membranes loaded with 2% bromelain showed full healing for the wounds, re-epithelialization and development of collagen fibres.[48] In addition, core–shell CS/PVA/alginate with asiaticoside enhanced wound closure (99.2 ± 1.11%) and developed new hairs after 21 days.[49] Moreover, CS/PVA nanofibers loaded with honey and *Nepeta dschuparensis* plant extract were reported for the treatment of second-degree burns.[50] The results revealed a high wound healing percentage (59.85 ± 0.14%) after 21 days. Saghafi *et al.* reported electrospun PCL/CS nanofibers that reduced the period of wound healing to 7 days.[51] The use of PCL with CS for wound healing was also reported in the form of a nanofibrous mat in a double-layered wound dressing loaded with propolis ethanolic extract, which induced complete wound healing within 15 days. The nanofibrous mat showed a well-formed dermis, growth of hair follicles, sebaceous glands, and structured collagen fibres on day 15.[52] In the current experimental work, plain PCL/CS core–shell NPs showed a burn diameter of 6.92 mm on day 21, confirming their participation in the wound healing process.

It is well known that significant levels of pro-inflammatory cytokines are released into the bloodstream following severe burns. In addition to disrupting the intestinal barrier, pro-inflammatory cytokines such as IL-13 and TNF-α also increase intestinal permeability.[53] In burns, researchers claim that TNF-α promotes the production of IL-13.[54] IL-13 is one of the powerful modulators of skin fibrosis and scarring. In the wound healing process, IL-13 promotes the proliferation and differentiation of fibroblasts, and triggers type I collagen expression.[55] In addition, IL-13 has several immune functions due to its transmitting activities, and it also regulates inflammation, fibrogenesis and allergic reactions.[56] A clinical study on burns showed an elevation in IL-13 levels, which might be attributed to activation of the immune system, where anti-inflammatory

and pro-inflammatory mediators are increased and prolonged for several months.[57]

TNF-α is a potential growth factor in the initial systemic response after burn injury. It is normally produced by mast cells, macrophages and neutrophils. This growth factor performs several effector immunological functions that are partly conflicting.[58] TNF-α induces apoptosis of many cell types, and contributes to the antimicrobial response. Epidermal burn damage promotes cell death due to chronic inflammation.[59] CS was involved in hydrogel formulation with hyaluronic acid, gelatine, zinc oxide, and copper oxide for the treatment of second-degree burns. This hydrogel showed a reduction in TNF-α levels after 7 days from burn induction, which became slower after 14 days.[60] Curcumin-encapsulated CS downregulates TNF-α expression, so it controls the pro-inflammatory response.[61] In the present study, G6 animals showed the highest level of TNF-α, whereas G3 showed the lowest level compared to G6 and G4 mice.

A previous study investigated the impact of TTO on the release of inflammatory mediators by activating blood monocytes with lipopolysaccharides (LPSs) *in vitro*. The findings suggested that certain components of TTO might be harmful to monocytes, whereas terpinen-4-ol, α-terpineol, and 1,8-cineole inhibit their release without significant toxicity. After 40 hours of incubation, the water-soluble constituents of TTO significantly reduced the levels of TNF-α, IL-10, IL-8, IL-1β and prostaglandin E2.[62,63]

T-cells are activated and undergo proliferation and development into effector or memory T cells. The activated $CD4^+$ T-cell subset is involved in orchestrating the adaptive immune response through releasing pro-inflammatory cytokines (*e.g.* IL-2, IFN-γ, and TNF-α), which are implicated in cell-mediated immunity. Additionally, $CD4^+$ T-cells release cytokines that influence the humoral immune response, such as IL-4, IL-10, and IL-13, as well as cytokines of T helper type 2 (Th2) cells.[53]

Following burn injury, $CD8^+$ T-cells are more observed than $CD4^+$ T-cells in the proliferation processes. Furthermore, compared to the proliferation of isolated $CD4^+$ T-cells, $CD8^+$ T-cell proliferation seems to be less dependent on other immune cells. The present study emphasized the significance of $CD8^+$ T-cells in the early immune response to second-degree burn injury.[64] Meanwhile, the study showed that $CD8^+$ T-cell subsets were more than $CD4^+$ T-cells in the G6 animals, which may contribute to the immune reaction after the burn in the early stage of the induction.

Previous results showed a reduction in the $CD4^+/CD8^+$ ratio in the burn area, and that double-negative T-cells may play a role in the pathophysiology of burn wounds. This mechanism may be ascribed to multiple factors and linked to alterations in growth factors, cytokines and haematological responses caused by burns. In order to reduce the initial inflammatory reaction to damage, the double-negative T-cells are a suitable option because they can prevent activation of myeloid cells and inhibit lymphocyte proliferation through cytokines of Th2 or suppressor myeloid cells. Moreover, it was suggested that T-cells may be important in regulating the transition from the inflammatory to tissue remodelling stages of wound healing.[65] In our study, the percentage frequency of the parent of $CD4^+/CD8^+$ in G6 animals was the lowest among all other animal groups, thus confirming the regulating effect of T-cells in wound healing.

A PCL/CS nanofibrous scaffold loaded with *Zataria multiflora*'s volatile oil showed a clear decrease in wound size on days 7, 14 and 21. The histological parameters on day 21 referred to the ability of these nanofibrous scaffolds to reduce vascularity, oedema and inflammation, while increasing re-epithelialization, collagen deposition and fibrosis.[66] Moreover, CS with glycosaminoglycan scaffolds in the burn model showed good histological results of complete epidermal layer formation and no inflammatory cell infiltration after 18 days.[67] Furthermore, a hydrogel of carboxymethyl CS and plantamajoside was reported for wound healing application. It was found that the hydrogel increased granulation tissues, stimulated collagen deposition and significantly enhanced re-epithelialization.[68] In another study, a mixture of CS and heparin was used to treat burns in the back of rats. The histological results revealed that the animals that received CS had lower burn injury than the control animal group, and that the used formulation reduced burn progress in the preliminary stage, after 72 h.[69] Furthermore, CS with high molecular weight showed the development of epithelialization and high formation of granular tissue in rat burns.[70] All the above-mentioned reports confirm the role of CS and PCL in accelerating second-degree burn healing as reported in the present study.

Conclusions

The present work described the fabrication and characterization of tea-tree oil loaded PCL/CS core–shell NPs for the treatment of second-degree burns. The work is a continuation of our previously published study devoted to *in vitro* characterization of the anti-microbial and anti-inflammatory activities of the same nano-formulation. The performed investigations revealed that the suggested TTO delivery system provided a novel, biocompatible, and effective potential treatment for second-degree burns in albino mice. It provided long-term anti-inflammatory anti-microbial activity, promoted tissue regeneration, induced haemostasis, and will have a good impact on improving the quality of life of second-degree burn patients. The drug delivery system suggested herein is applied topically using a cream formulation, and acts as an effective and fast cure for burns, as well as reducing the economic burden of their treatment.

Author contributions

AHS: investigation, methodology, data analysis, visualization, writing-original draft. AMB: writing-review and editing, supervision, resources. ZAM: methodology, investigation, analysis, resources. MEAZ: methodology, investigation, analysis, resources. AAK: investigation, writing-review and editing. NAM: writing-review and editing, supervision, resources. ASAD: conceptualization, methodology, investigation, data analysis,

visualization, writing-review and editing, project administration.

Conflicts of interest

There are no conflicts to declare.

Data availability

All the data required to support the findings of this manuscript are included in the main text.

Supplementary information is available. See DOI: https://doi.org/10.1039/d5na00391a.

Notes and references

1 F. N. Williams, D. N. Herndon, H. K. Hawkins, J. O. Lee, R. A. Cox, G. A. Kulp, C. C. Finnerty, D. L. Chinkes and M. G. Jeschke, *Crit. Care*, 2009, **13**, R183.
2 M. G. Jeschke, M. E. van Baar, M. A. Choudhry, K. K. Chung, N. S. Gibran and S. Logsetty, *Nat. Rev. Dis. Primers*, 2020, **6**, 11.
3 W. Żwierełło, K. Piorun, M. Skórka-Majewicz, A. Maruszewska, J. Antoniewski and I. Gutowska, *Int. J. Mol. Sci.*, 2023, **24**, 3749.
4 R. Warby, C. V. Maani, *StatPearls*, 2023, https://www.ncbi.nlm.nih.gov/books/NBK539773/, accessed October 28, 2025.
5 J. Oh, C. Madison, G. Flott, E. G. Brownson, S. Sibbett, C. Seek, G. J. Carrougher, C. M. Ryan, K. Kowalske, N. S. Gibran and B. T. Stewart, *J. Burn Care Res.*, 2021, **42**, 1110.
6 S. Ji, S. Xiao, Z. Xia and C.-S. M. E. A. of C. Chinese Burn Association Tissue Repair of Burns and Trauma Committee, *Burns Trauma*, 2024, **12**, tkad061.
7 B. M. Parrett, B. Pomahac, R. H. Demling and D. P. Orgill, *J. Burn Care Res.*, 2006, **27**, 34–39.
8 S. C. Pan, *Burns Trauma*, 2013, **1**, 27–31.
9 R. N. Odondi, R. Shitsinzi and A. Emarah, *Heliyon*, 2020, **6**, e03629.
10 Z. G. Chukamei, M. Mobayen, P. B. Toolaroud, M. Ghalandari and S. Delavari, *Int. J. Burns Trauma*, 2021, **11**, 397.
11 C. F. Carson, K. A. Hammer and T. V. Riley, *Clin. Microbiol. Rev.*, 2006, **19**, 50.
12 T. Nascimento, D. Gomes, R. Simões and M. da Graça Miguel, *Antioxidants*, 2023, **12**, 1264.
13 L. Kairey, T. Agnew, E. J. Bowles, B. J. Barkla, J. Wardle and R. Lauche, *Front. Pharmacol*, 2023, **14**, 1116077.
14 M. N. M. Nogueira, S. G. Aquino, C. Rossa and D. M. P. Spolidorio, *Inflammation Res.*, 2014, **63**, 769–778.
15 P. H. Hart, C. Brand, C. F. Carson, T. V. Riley, R. H. Prager and J. J. Finlay-Jones, *Inflammation Res.*, 2000, **49**, 619–626.
16 A. Bugarcic, E. J. Bowles, K. Summer, T. Agnew, B. Barkla and R. Lauche, *Phytomed. Plus*, 2025, **5**, 100846.
17 J. Zhao, P. Qiu, Y. Wang, Y. Wang, J. Zhou, B. Zhang, L. Zhang and D. Gou, *Int. J. Biol. Macromol.*, 2023, **244**, 125250.
18 A. Moeini, P. Pedram, P. Makvandi, M. Malinconico and G. Gomez d'Ayala, *Carbohydr. Polym.*, 2020, **233**, 115839.
19 Z. Hu, J. Shan, X. Jin, W. Sun, L. Cheng, X. L. Chen and X. Wang, *ACS Nano*, 2024, **18**, 24327–24349.
20 W. Wang, Y. Cui, X. Wei, Y. Zang, X. Chen, L. Cheng and X. Wang, *ACS Nano*, 2024, **18**, 15845–15863.
21 Y. Sun, W. Zhang, Z. Luo, C. Zhu, Y. Zhang, Z. Shu, C. Shen, X. Yao, Y. Wang and X. Wang, *Adv. Funct. Mater.*, 2025, **35**, 2415778.
22 X. Feng, Z. Luo, W. Zhang, R. Wan, Y. Chen, F. Li, Y. He, Z. Lin, J. H. Hui, J. Conde, S. Chen, Z. Zhao and X. Wang, *Adv. Funct. Mater.*, 2025, **35**, 2506476.
23 X. Zhou, H. Wang, J. Zhang, X. Li, Y. Wu, Y. Wei, S. Ji, D. Kong and Q. Zhao, *Acta Biomater.*, 2017, **54**, 128–137.
24 A. H. Saleh, A. M. Badr, Z. A. Muhammad, M. E. A. Zaki, A. E. Abdelkader, N. A. Mahana and A. S. A. Dena, *Bionanoscience*, 2025, **15**, 1–11.
25 S. S. Priyadarsini, P. R. Kumar and M. Thirumal, *Int. J. Green Pharm.*, 2018, **12**, S537–S542.
26 K. S. Priya, A. Gnanamani, N. Radhakrishnan and M. Babu, *J. Ethnopharmacol.*, 2002, **83**, 193–199.
27 M. Hazrati, D. Mehrabani, A. Japoni, H. Montasery, N. Azarpira, A. R. Hamidian-Shirazi and N. Tanideh, *J. Appl. Anim. Res.*, 2010, **37**, 161–165.
28 G. Lin, H. Chen, H. Zhou, X. Zhou and H. Xu, *Materials*, 2018, **11**(5), 710.
29 G. Rytwo, R. Zakai and B. Wicklein, *J. Spectrosc.*, 2015, **2015**, 727595.
30 K. Kalwar, W.-X. Sun, D.-L. Li, X.-J. Zhang and D. Shan, *React. Funct. Polym.*, 2016, **107**, 87–92.
31 S. A. Blome-Eberwein, H. Amani, D. D. Lozano, C. Gogal, D. Boorse and P. Pagella, *Burns*, 2021, **47**, 838–846.
32 M. Kurakula, G. S. N. K. Rao and K. S. Yadav, *Applications of Advanced Green Materials*, 2020, pp. 395–423.
33 N. K. Varde and D. W. Pack, *Expet Opin. Biol. Ther.*, 2004, **4**, 35–51.
34 Z. S. Haidar, *Polymers*, 2010, **2**, 323–352.
35 F. C. Flores, J. A. de Lima, R. F. Ribeiro, S. H. Alves, C. M. B. Rolim, R. C. R. Beck and C. B. da Silva, *Mycopathologia*, 2013, **175**, 281–286.
36 R. Ekambaram, M. Sugumar, S. Karuppasamy, P. Prasad and S. Dharmalingam, *J. Drug Deliv. Sci. Technol.*, 2022, **71**, 103286.
37 S. Zamani and S. Khoee, *Polymer*, 2012, **53**, 5723–5736.
38 P. Huang, C. Yang, J. Liiu, W. Wang, S. Guo, J. Li, Y. Sun, H. Dong, L. Deng, J. Zhang, J. Liu and A. Dong, *J. Mater. Chem. B*, 2014, **2**, 4021–4033.
39 N. P. da Silva, E. do Carmo Rapozo Lavinas Pereira, L. M. Duarte, J. C. de Oliveira Freitas, C. G. de Almeida, T. P. da Silva, R. C. N. de Melo, A. C. M. Apolônio, M. A. L. de Oliveira, H. de Mello Brandão, F. Pittella, R. L. Fabri, G. D. Tavares and P. de Faria Pinto, *Colloids Surf., B*, 2020, **196**, 111371.

40 R. Grillo, N. Z. P. dos Santos, C. R. Maruyama, A. H. Rosa, R. de Lima and L. F. Fraceto, *J. Hazard. Mater.*, 2012, **231–232**, 1–9.
41 H. Y. Atay, Antibacterial Activity of Chitosan-Based Systems, in *Functional Chitosan*, ed. S. Jana and S. Jana, Springer, Singapore, 2019, DOI: 10.1007/978-981-15-0263-7_15.
42 J. Zhang, C. He, C. Tang and C. Yin, *Pharm. Res.*, 2013, **30**, 1228–1239.
43 R. Kamel, S. M. Afifi, A. M. Abdou, T. Esatbeyoglu and M. M. AbouSamra, *Molecules*, 2022, **27**, 1–19.
44 R. Ramalingam, C. Dhand, V. Mayandi, C. M. Leung, H. Ezhilarasu, S. K. Karuppannan, P. Prasannan, S. T. Ong, N. Sunderasan, I. Kaliappan, M. Kamruddin, V. A. Barathi, N. K. Verma, S. Ramakrishna, R. Lakshminarayanan and K. D. Arunachalam, *ACS Appl. Mater. Interfaces*, 2021, **13**, 24356–24369.
45 F. Doustdar, S. Ramezani, M. Ghorbani and F. M. Moghadam, *Int. J. Pharm.*, 2022, **627**, 122218.
46 T. L. Kennewell, S. Mashtoub, G. S. Howarth, A. J. Cowin and Z. Kopecki, *Wound Pract. Res.*, 2019, **27**, 175–183.
47 R. Augustine, E. A. Dominic, I. Reju, B. Kaimal, N. Kalarikkal and S. Thomas, *RSC Adv.*, 2014, **4**, 24777–24785.
48 S. Bayat, N. Amiri, E. Pishavar, F. Kalalinia, J. Movaffagh and M. Hashemi, *Life Sci.*, 2019, **229**, 57–66.
49 L. Zhu, X. Liu, L. Du and Y. Jin, *Biomed. Pharmacother.*, 2016, **83**, 33–40.
50 A. Naeimi, M. Payandeh, A. R. Ghara and F. E. Ghadi, *Carbohydr. Polym.*, 2020, **240**, 116315.
51 Y. Saghafi, H. Baharifar, N. Najmoddin, A. Asefnejad, H. Maleki, S. M. Sajjadi-Jazi, A. Bonkdar, F. Shams and K. Khoshnevisan, *Gels*, 2023, **9**, 672.
52 M. S. Karizmeh, S. A. Poursamar, A. Kefayat, Z. Farahbakhsh and M. Rafienia, *Biomater. Adv.*, 2022, **135**, 112667.
53 L. Boldeanu, M. Boldeanu, M. Bogdan, A. Meca, C. Coman, B. Buca, C. Tartau and L. Tartau, *Exp. Ther. Med.*, 2020, 2361–2367.
54 L. T. Sun, E. Friedrich, J. L. Heuslein, R. E. Pferdehirt, N. M. Dangelo, S. Natesan, R. J. Christy and N. R. Washburn, *Wound Repair Regen.*, 2012, **20**, 563.
55 J. K. Nguyen, E. Austin, A. Huang, A. Mamalis and J. Jagdeo, *Arch. Dermatol. Res.*, 2020, **312**, 81–92.
56 E. Roeb, *Int. J. Mol. Sci.*, 2023, **24**, 12884.
57 M. Carlton, J. Voisey, T. J. Parker, C. Punyadeera and L. Cuttle, *Burns Trauma*, 2021, **9**, tkaa049.
58 H. I. Korkmaz, G. Flokstra, M. Waasdorp, A. Pijpe, S. G. Papendorp, E. de Jong, T. Rustemeyer, S. Gibbs and P. P. M. van Zuijlen, *Cells*, 2023, **12**, 345.
59 C. B. Nielson, N. C. Duethman, J. M. Howard, M. Moncure and J. G. Wood, *J. Burn Care Res.*, 2017, **38**, e469–e481.
60 A. V. Thanusha, A. K. Dinda and V. Koul, *Mater. Sci. Eng., C*, 2018, **89**, 378–386.
61 F. Li, Y. Shi, J. Liang and L. Zhao, *J. Biomater. Appl.*, 2019, **34**, 476–486.
62 P. H. Hart, C. Brand, C. F. Carson, T. V. Riley, R. H. Prager and J. J. Finlay-Jones, *Inflammation Res.*, 2000, **49**, 619–626.
63 G. Sandner, M. Heckmann and J. Weghuber, *Biomolecules*, 2020, **10**, 1–16.
64 I. B. Buchanan, R. Maile, J. A. Frelinger, J. H. Fair, A. A. Meyer and B. A. Cairns, *J. Trauma*, 2006, **61**, 1062–1068.
65 M. Rani and M. G. Schwacha, *PLoS One*, 2017, **12**, 4–15.
66 M. Osanloo, F. Noori, N. Varaa, A. Tavassoli, A. Goodarzi, M. T. Moghaddam, L. Ebrahimi, Z. Abpeikar, A. R. Farmani, M. Safaei, N. Fereydouni and A. Goodarzi, *BMC Complementary Med. Ther.*, 2024, **24**, 1–16.
67 G. Sandri, S. Rossi, M. C. Bonferoni, D. Miele, A. Faccendini, E. Del Favero, E. Di Cola, A. I. Cornaglia, C. Boselli, T. Luxbacher, L. Malavasi, L. Cantu and F. Ferrari, *Carbohydr. Polym.*, 2019, **220**, 219–227.
68 N. Yu, Y. Li, Y. Wang, H. Xu, F. Ye and Q. Fu, *Burns*, 2022, **48**, 902–914.
69 Y. Jin, P.-X. Ling, Y.-L. He and T.-M. Zhang, *Burns*, 2007, **33**, 1027–1031.
70 I. A. Alsarra, *Int. J. Biol. Macromol.*, 2009, **45**, 16–21.